Optical Materials 86 (2018) 414–420

Contents lists available at ScienceDirect

Optical Materials

journal homepage: www.elsevier.com/locate/optmat

Intrinsic five-photon non-linear absorption of two-dimensional BN and its conversion to two-photon absorption in the presence of photo-induced defects

Yongchang Dong[a], Prakash Parajuli[a], Apparao M. Rao[a,b], Wim Thielemans[c], Samuel Eyley[c], Krishna Rani Sahoo[d], T.N. Narayanan[d], Ramakrishna Podila[a,b,*]

[a] Department of Physics and Astronomy, and Clemson Nanomaterials Institute, Clemson, SC, 29634, USA
[b] Clemson Laboratory of Nano-biophysics, Clemson University, Clemson, SC, 29634, USA
[c] Renewable Materials and Nanotechnology Research Group, Department of Chemical Engineering, KU Leuven Kortrijk Kulak Campus, Etienne Sabbelaan 53 Box 7659, 8500, Kortrijk, Belgium
[d] Tata Institute of Fundamental Research (TIFR), Hyderabad, 500045, India

ARTICLE INFO

Keywords:
Boron nitride
Two-dimensional materials
Nonlinear optical properties
Z-scan
Multiphoton absorption*Keywords:*
Boron nitride
Two-dimensional materials
Non-linear optics
Multi-photon absorption
Defects
X-ray photoemission spectroscopy

ABSTRACT

Unlike most two-dimensional materials, h-BN nanoplatelets (BNNPs) exhibit multi-photon absorption. This was previously attributed to a two-photon absorption (2PA) process at 1.16 eV by Kumbhakar et al., Advanced Optical Materials, 3, 828, 2015. This is counter-intuitive because a 2PA process at 1.16 eV cannot excite electrons across the wide band gap of BNNPs (~5.75 eV). Here, through systematic experimental and theoretical work, we provide compelling evidence that BNNPs exhibit five-photon absorption (5PA) at a low-laser fluence (< 0.6 J/cm^2). Furthermore, we show that a high laser fluence (> 0.6 J/cm^2) generates photo-induced defects in BNNPs that support a 2PA process. Accordingly, we assert that BNNPs inherently exhibit 5PA at a low laser fluence. In the previous study reported by Kumbhakar et al. a high laser fluence was used, which led to the observation of 2PA process.

1. Introduction

Two–dimensional (2D) materials exhibit unique optical properties that are different from their bulk. A testament to this fact is the increasing use of 2D materials in solar cells, light-emitting devices, photodetectors, and ultrafast lasers [1–4]. An interesting feature of light-matter interactions in many 2D materials [5–7] (*e.g.*, graphene, transition metal dichalcogenides, and phosphorene) is their increased transparency at higher light input fluences or the so-called nonlinear saturable absorption (SA) [7–10]. The SA phenomenon is a direct consequence of dynamical interactions between electrons in 2D materials with the incident laser pulses, which allow for resonant or near-resonant excitation through single-photon absorption [7–10]. In many 2D materials, the excited state absorption cross-section was experimentally found to be lower than that of the ground state absorption [8,11–14]. Consequently, the absorption saturates at an input fluence that is sufficiently high for bleaching the ground state electrons. While this phenomenon is well-known in bulk materials (*e.g.*, Cr:YAG), the threshold SA fluence of 2D materials is significantly higher: a critical requirement for ultrafast laser pulse shaping. Many 2D materials (*e.g.*, graphene and MoS_2) are now being used as SA in mode locking and pulse-shaping in ultrafast lasers [6,13,15,16]. Interestingly, other intriguing nonlinear optical effects such as multi-photon or reverse saturable absorption, often exhibited by other nanomaterials (*e.g.*, C_{60} [7,10], metal-oxide nanoparticles [17–19]) are rarely observed in the nonlinear optical (NLO) properties of undoped 2D materials. Nevertheless, doped 2D materials (*e.g.*, BCN [20]) show multi-photon absorption.

The recent realization of single/few-layer h-BN, which is an isostructural cousin to graphene with a wide band gap of ~5.5–6 eV [21], has opened new vistas for studying multiphoton absorption (MPA) in 2D materials. Previously, Kumbhakar et al. [22] reported a strong two photon absorption (2PA) in few-layer h-BN sheets when exposed to nanosecond pulses of a Nd:YAG at 1064 nm (corresponding to a single-photon energy of ~1.16 eV). This effect was attributed to the large transition dipole moment resulting from the electronegativity

* Corresponding author. Clemson Laboratory of Nano-biophysics, Clemson University, Clemson, SC, 29634, USA.
E-mail address: rpodila@g.clemson.edu (R. Podila).

https://doi.org/10.1016/j.optmat.2018.10.022
Received 17 August 2018; Received in revised form 9 October 2018; Accepted 13 October 2018

difference between B and N atoms. Furthermore, they reported an anomalously large value for 2PA cross-section at 1064 nm: ~52 times larger than the well-known efficient squaraine-bridged porphyrin dimer [23]. From a theoretical standpoint, h-BN should exhibit five-photon absorption (or 5PA) when excited with 1064 nm excitation via the simultaneous absorption of five photons corresponding to an energy ~5.80 eV. Given that the band gap of h-BN is ~5.5–6 eV, the conclusions from Kumbhakar et al. [22] are peculiar because the energy of two photons from a 1064 nm Nd:YAG laser (two-photon energy ~2.32 eV) is insufficient to excite electrons across the band gap. Thus, a fundamental understanding of the nonlinear light-matter interactions in h-BN is still lacking.

Materials exhibiting a 5PA process (either at the bulk or nanoscale) have rarely been investigated in the literature due to the extremely low transition probability associated with a 5PA process [24–26]. Often, the necessary fluence for eliciting 5PA in most materials using nanosecond pulses is well beyond the output of conventional lasers. In this study, we show that pristine h-BN nanoplatelets (BNNPs) inherently exhibit a high transition probability for 5PA when excited with 7 ns pulses of 1064 nm. Thus, BNNPs provide a unique platform for studying exquisite higher-order nonlinearities such as 5PA at low laser fluences (~0.2 J/cm^2) accessible through a ns pulsed Nd:YAG laser. Moreover, it is well known that MPA at higher fluence can either initiate photo-polymerization at the microscopic scale [27] or induce defects in the material under study via multiphoton ionization [28]. In case of BNNPs, we observed that a suspension of BNNPs in isopropyl alcohol (IPA) photo-transforms into doped BNNPs with altered configurations of N atoms when excited by a 1064 nm laser at high fluence. While BNNPs inherently exhibited 5PA at a low laser fluence (< 0.6 J/cm^2), they instantaneously undergo photo-transformation at a high laser fluence leads to 2PA. We used finite-element methods (COMSOL Multiphysics) to uncover that the high laser fluence raises the temperature of BNNPs to ~960 °C, which consequently promotes doping at the edge sites of BNNPs. In a separate experiment, we prepared O/C doped BNNPs via an alternate route, such as the high-energy ball-milling process, to confirm the influence of laser-induced transformation of the NLO properties in BNNPs, *viz.*, the switching from 5PA to 2PA. Moreover, a clear evidence for the laser-induced doping which promotes the formation of B—O and C—N bonds was elicited through x-ray photoelectron spectroscopy (XPS) of photo-transformed BNNPs. Lastly, the O/C induced electronic states obtained from our density-functional theory (DFT) calculations, provide a rational explanation for the experimentally observed switching in the NLO properties of BNNPs at high laser fluences.

2. Experimental section

Dispersion of BNNPs: Hexagonal boron nitride powder (1 μm, 98%) was purchased from Sigma Aldrich. They were exfoliated the using a tip sonicator (Branson, 250 W) with ~3 mg/ml concentration in *N*-methyl pyrrolidone (NMP). After exfoliation, the samples were centrifuged at 3000 rpm and the supernatant was collected and washed at least thrice with DI water. The BNNPs for Z-scan experiments (~1 mg/ml) were dispersed in IPA using a aqueous bath sonicator (Branson Aquasonic) for 5 min. Such dispersions were found to be stable for more than an hour, which enabled collection of reliable Z-scans for evaluating the NLO properties of BNNPs.

Sample preparation of ball milled BNNPs: For preparing doped BNNPs, two methods were used, *viz.*, ball milling and chemical vapor deposition (CVD). For milling, BNNPs were ball milled with graphite (9:1 wt ratio) in a high-energy ball mill machine (MSK-SFM-3, MTI Corp.) for 2 h. The CVD process was carried out on a different set of BNNPs in a quartz tube reactor (length 120 cm, and inner diameter 4.5 cm) at atmospheric pressure using CH_4 gas as carbon source. About 50 mg of exfoliated hBN (powder form of hBN kept inside an alumina boat covered with copper foil) was heated to 1000 °C for 60 min in 200 standard cubic centimeters per minute (sccm) Ar/H_2 flow. Next, the CH_4 gas flow is introduced (50 sccm) for 15 min in the presence of the Ar/H_2 flow. Subsequently, the CH_4 gas and the CVD furnace were turned off, and the furnace allowed to cool down rapidly (by opening the clam-shell furnace) to room temperature in flowing 200 sccm Ar/H_2.

Characterization: Raman spectroscopy was performed using a Renishaw in Via Raman microscope equipped with a diode pumped laser source of 532 nm (CrystalLaser, Inc). High resolution X-ray diffraction (HR-XRD) was performed using a RIGAKU Ultima IV diffractometer, Cu Kα radiation, k ¼ 1.5406 Å on powder samples that were held in a standard Al sample holder. Quantitative analysis using Rietveld refinement was performed on the XRD peaks using PDXL software. TEM images were obtained using a Hitachi H-9500. While some preliminary XPS studies were performed using a Kratos Axis Ultra DLD instrument (calibrated by the C1s line present at 284.6 eV), more detailed XPS results on CVD-doped BN were obtained using a Kratos Axis Supra XPS employing a monochromated Al K_α ($h\nu$ = 1486.7 eV, 10 mA emission) x-ray source, hybrid (magnetic/electrostatic) optics with a slot aperture, hemispherical analyser, multichannel plate and delay line detector (DLD) with a take-off angle of 90°. High resolution spectra were taken with a pass-energy of 20 eV CVD doped BN was conducting during XPS data acquisition and data were collected with the sample in electrical contact with the spectrometer. Binding energy was referenced to Au4$f_{7/2}$ at 83.96 eV as measured just prior to the sample data acquisition. Quantification was performed using empirical relative sensitivity factors supplied by Kratos Analytical (Manchester, UK).

Z-scan technique: In our Z-scan setup (see Fig. S1), a linearly polarized 7 ns optical pulsed beam from a Q-switched frequency-doubled 1064 nm Nd:YAG laser was focused by a converging lens (focal length of ~20 cm) to form an optical field of gradually changing laser intensity. A LabVIEW program synchronized the single-shot laser pulses with the moving stage and the resulting repetition rate was ~1 Hz. The linear absorption of BNNP dispersions was quantified using a UV-Vis spectrometer (Perkin Elmer, Lambda) (Fig. S2), which showed an increased absorption below 400 nm peaked (~225–240 nm) concomitant with the band gap of BNNPs ~5.5 ± 0.5 eV. The linear transmittance (1 mg/ml) at 1064 nm was found to be ~75% at 1064 nm for 1 mg/ml BN dispersions in IPA. The BNNPs/IPA dispersions were held in 1 mm thick quartz cuvettes (100-QS Hellma® Analytics) and translated across the focal plane in the beam direction (Z-direction). With the sample dispersions experiencing different optical intensities at each *z* position, the corresponding transmittance was recorded by a calibrated photodetector D2 RjP-7620, Laserprobe, Inc.) placed on the sample translation axis (see Fig. S1). A photodetector was placed off-axis for obtaining nonlinear scattering data. A detailed description of the Z-scan technique can be found elsewhere [7,10,16,29–33].

In our experiments, the open aperture Z-scan MPA coefficients were calculated from spectra under the assumption that only one type of MPA dominates at any given time. The optical intensity *I* can be described as [21].

$$\frac{dI}{dz'} = -\alpha_N I^{N-1} \tag{1}$$

where *z'* is propagation distance of light within the sample and α_N is the *N*-photon absorption coefficient. For example, α_2 represents the 2PA coefficient while α_5 denotes 5PA. The obtained Z-scan data was fitted by numerically solving equation (1) in MATLAB. A fit was deemed good for R^2 (coefficient of determination) values > 0.9.

3. Results

BNNPs (Sigma Aldrich) were characterized by XRD, Raman spectroscopy, TEM and XPS. The four XRD peaks at ~26°, ~42°, ~50° and ~55° (Fig. 1) are due to diffraction from the (002), (100), (102) and (004) planes, and the additional diffraction peaks at ~38° and ~44° stem from the Al sample holder. A lattice constant of 3.29 Å was

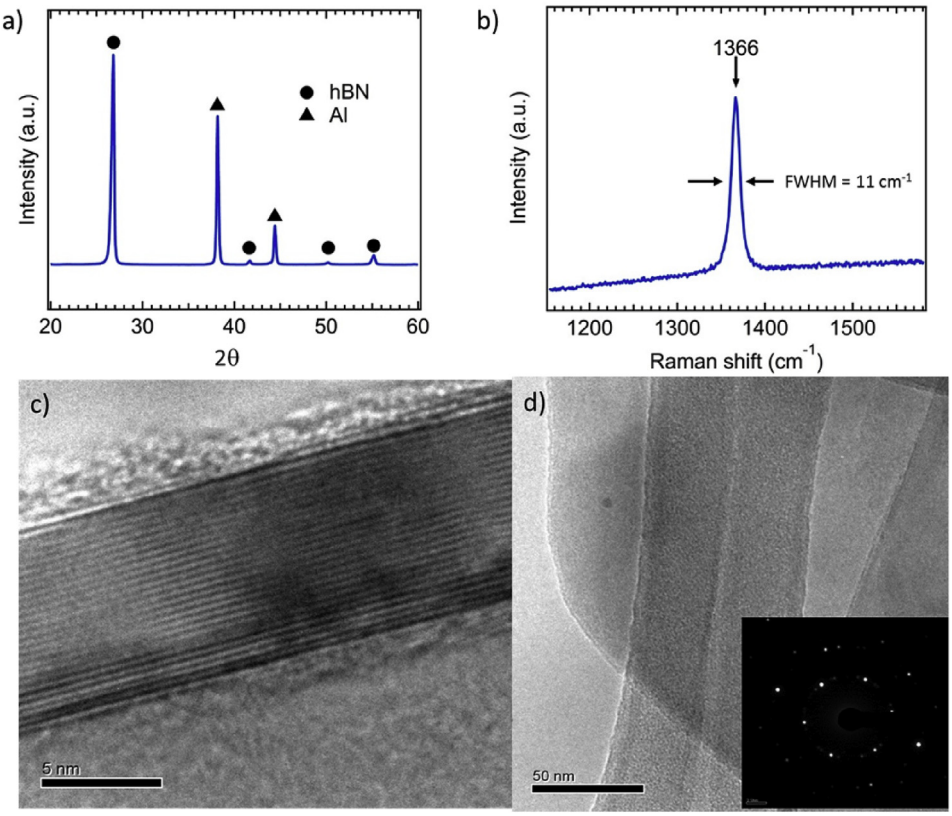

Fig. 1. a) XRD pattern of BNNPs held on an Al sample holder. b) Raman spectrum of pristine BNNPs using the 532 nm laser excitation. HRTEM images of BNNPs c) side view and d) top view. The inset of d) is the selected area electron diffraction of the BNNP.

deduced from the pattern in Fig. 1a for BNNPs, and its Raman spectrum (Fig. 1b) showed the characteristic E_{2g} band at 1366 cm^{-1} (FWHM = 11 cm^{-1}). The dynamic light scattering (DLS) measurements (Nanosizer S90, Malvern Instruments) revealed a lateral size of BNNPs as 745 ± 92 nm. HRTEM images of the BNNPs are shown in Fig. 1c and d. We found that BNNPs were an average of ~20–25 layers in thickness which exhibited a hexagonal electron diffraction pattern indicating high crystallinity.

We used the open aperture Z-scan method (see experimental section and Fig. S1 for a detailed description) for investigating the NLO properties of BNNPs (suspended in IPA) under varying 1064 nm (1.16 eV) laser fluences. The UV-Vis spectrum of BNNP is shown in Fig. S2. Fig. 2a shows a typical normalized transmission (T/T_0, where T and T_0 are the nonlinear and linear transmittance values) curve for BNNPs when excited with a laser energy of ~220 μJ (corresponding to a fluence of ~0.4 J/cm^2 at the focal point), which could be best fit to a 5PA process (see solid trace in Fig. 2a and Fig. S3). This observation suggests that the electrons at the valence band maximum in BNNPs (band gap of 5.5–6 eV [34], also as observed from Fig. S2) can be excited to the conduction band through 5PA at input energies ~220 μJ. It should be mentioned that the possibility of nonlinear light scattering (NLS) leading to the response in Fig. 2a was ruled out by measuring the off-axis scattered light intensities (see Supplementary Information Fig. S4). Interestingly, when the laser fluence was increased to ~350 μJ (corresponding to a fluence of ~0.6 J/cm^2 at the focal point), an abrupt change in the lineshape of BNNPs' normalized transmittance past the focal point (z = 0 mm) became evident (Fig. 2b). The pre-focus Z-scan data for 350 μJ in Fig. 2b, obtained as the sample approached the focal point (see blue arrow in Fig. S1), was best fitted to 5PA. However, the past-focus data (receding from the focal point, green arrow in Fig. S1) showed the presence of two-photon absorption or 2PA.

In reality, BNNPs support 5PA as long as the input fluence is below the threshold value 0.6 ± 0.012 J/cm^2 - an inherent property of BNNPs which was overlooked in the study reported by Kumbhakar et al.

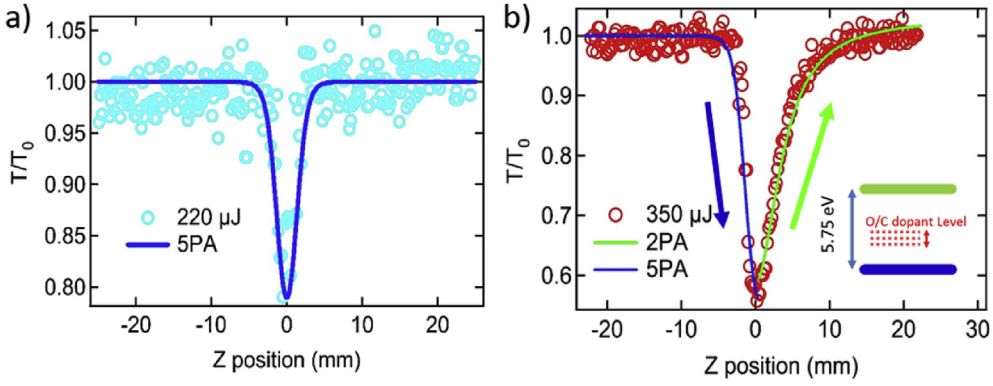

Fig. 2. a) A dispersion of pristine BNNPs in IPA exhibits a 5PA response in a Z-scan curve collected with a laser fluence of 220 μJ b) Upon increasing the laser fluence to 350 μJ, a 5PA response is observed, signaling an onset of photo-induced doping of BNNPs with carbon from the IPA. The coefficients for 2PA and 5PA found from the numerical fits (R^2 > 0.9) were 12 cm GW^{-1} and 2500 cm^7 GW^{-4}, respectively. A schematic inset showing the O/C dopant levels introduced into the wide band gap of h-BN. The presence of such levels at ~2–2.5 eV enable 2PA in the photo-transformed BNNPs.

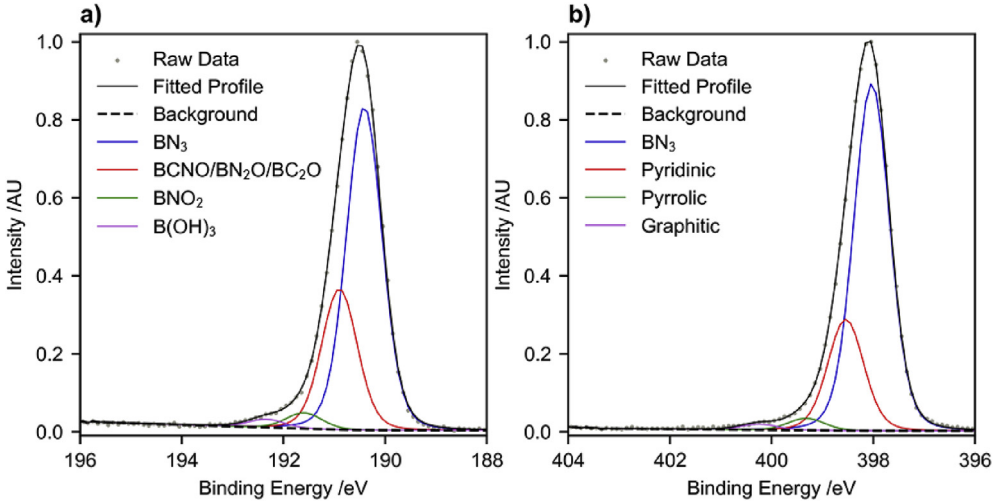

Fig. 3. a) and b) show B 1s and N1s XPS spectra for CVD doped BN. In both the cases, different environments were found as shown by the deconvoluted peaks. A complete list of peak positions and intensities in provided in Table S1.

due to the high fluence (3.9 J/cm^2, 1064 nm) used in their study. Furthermore, BNNPs are also expected to have mid-gap states within the band gap due to inherent defects that could provide real electronic states to support simultaneous 5PA in addition to spontaneous 5PA. However, we found that the 5PA co-efficient was the same at different intensities suggesting the inherent 5PA is virtual with simultaneous absorption. Given that the laser beam radius at the focal point was ~100 μm, only a small amount of BNNPs within the beam path is expected be photo-transformed. To confirm this, we repeated the Z-scan on the same BNNPs dispersion after gently stirring it. As expected, the inherent 5PA response of BNNPs was recovered (Fig. S5) implying that photo-transformed BNNPs were no longer present in the beam path. Also, no discernible changes were observed in the linear absorption spectrum before and after laser exposure. Furthermore, as mentioned earlier, we ruled out NLS effects arising from micro-bubbles at high laser fluence by using an off-axis detector (see Figs. S1 and S4). Based on the data presented in Fig. 2, we conclude that the much higher laser fluence used in the previous study by Kumbhakar et al. [22] (3.9 J/cm^2, 1064 nm) precluded the authors from uncovering the inherent 5PA in h-BN.

4. Discussion

We hypothesize that the high laser fluence promotes heteroatomic doping of oxygen/carbon (from IPA) into BNNPs, possibly at the edge sites due to its low formation energy [35,36]. The presence of O/C dopants in BN lattice is known to introduce new electronic states within the band gap [37–41], which could explain the observation of 2PA at high laser fluences [20]. Indeed, recent spectroscopic studies (cathodo- and photo-luminescence, UV absorption, and scanning tunneling spectroscopy) on defected/doped h-BN crystals and nanostructures found clear spectral features at lower energies (~2–4 eV) in addition to the band gap ~5.75 eV due to the presence of dopant-induced electronic states [41,42] within the band gap. Similarly, our theoretical studies using density functional theory (see Fig. S6) along with earlier investigations employing local density approximation and GW approximation confirmed the presence mid-gap states for C/O dopants at ~1–4 eV. Based on our Z-scan results and existing spectroscopic studies [7,10,43,44], we posit that the ground state electrons in doped BNNPs when excited with 1064 nm (or ~1.16 eV) photons are promoted to the C/O-dopant induced states present ~2–2.5 eV through a 2PA process (inset in Fig. 2b).

We used finite-element method (COMSOL Multiphysics) with a heat transfer module to simulate the conditions at high laser fluence that could result in doping of O/C into BNNPs. The BNNPs were modeled as platelets with average dimensions 100 × 100 × 10 nm^3 (as gleaned from TEM images such as the one presented in Fig. 1c) and the laser fluence was matched to threshold values for eliciting a 2PA response, *i.e.*, ~7 ns pulse with an energy density of ~0.6 J/cm^2 (*cf.* Fig. 2b). The temperature distribution of the BNNP platelets after exposure to a single laser pulse is shown in Fig. S7. Our COMSOL simulation revealed that the laser rapidly (~7 ns) heats the surface of the BNNP and increases its temperature to 950–966 °C. The top surface edges of the BNNP were raised to a higher temperature relative those on the bottom layer because the heat diffusion rate is much faster in the lateral (6 W cm^{-1} °C^{-1}) than in the vertical (0.3 W cm^{-1} °C^{-1}) direction for h-BN [45]. The laser-induced increase in the temperature at the edges of BNNP platelets is much higher than the decomposition temperature of IPA (~400 °C), which possibly leads to IPA carbonization and subsequent doping of BNNPs with carbon at its edge sites.

While conventional XPS is an excellent tool for confirming the presence of dopants in BNNPs, it is plagued by the presence of O/C peak of the IPA solvent used in this study. Moreover, only a small amount of BNNPs that are present within the beam path are photo-transformed. Thus, to confirm our hypothesis that BNNPs switch their NLO properties from 5PA to 2PA due to laser-induced doping of it edges with O/C, we intentionally doped BNNPs with O/C by two different methods: 1) CVD method with temperatures ~1000 °C as observed in the COMSOL simulation and 2) ball milling a mixture of BNNPs and graphite powder.

We performed detailed XPS studies on both CVD doped and ball-milled samples to ascertain different bonding environments (B—N, B—C, C—N, *N*—O, B—O etc) that could induce mid-gap states responsible for 2PA at higher fluence. In the case of CVD-doped BN (labeled CBN), its B 1s spectrum (Fig. 3a) exhibits at least four different environments. The lowest binding energy at 190.5 eV is assigned to B bonded to three N atoms. The lack of lower binding energy components in any of the samples is indicative of a lack of boron bonded to carbon and nitrogen alone. The higher binding energy components at 191.0 eV, 191.5 eV and 192 eV are tentatively ascribed to $BCNO/BN_2O/BC_2O$, BNO_2 and $B(OH)_3$ based on previously published XPS data for boron nitride systems [46–48]. The overall shape of the B 1s peak in all of these samples lacks structure and appears slightly asymmetric. Similar to the B 1s peak, the N 1s spectrum for CBN exhibited four different environments (Fig. 3b). The first environment at 398 eV is assigned to nitrogen bonded to boron. The other environments at 398.5 eV, 399 eV and 400 eV could be assigned to various bonding modes of carbon with nitrogen, referred to as pyridinic and pyrrolic and graphitic respectively [38,49]. These assignments are at slightly lower binding energies compared with

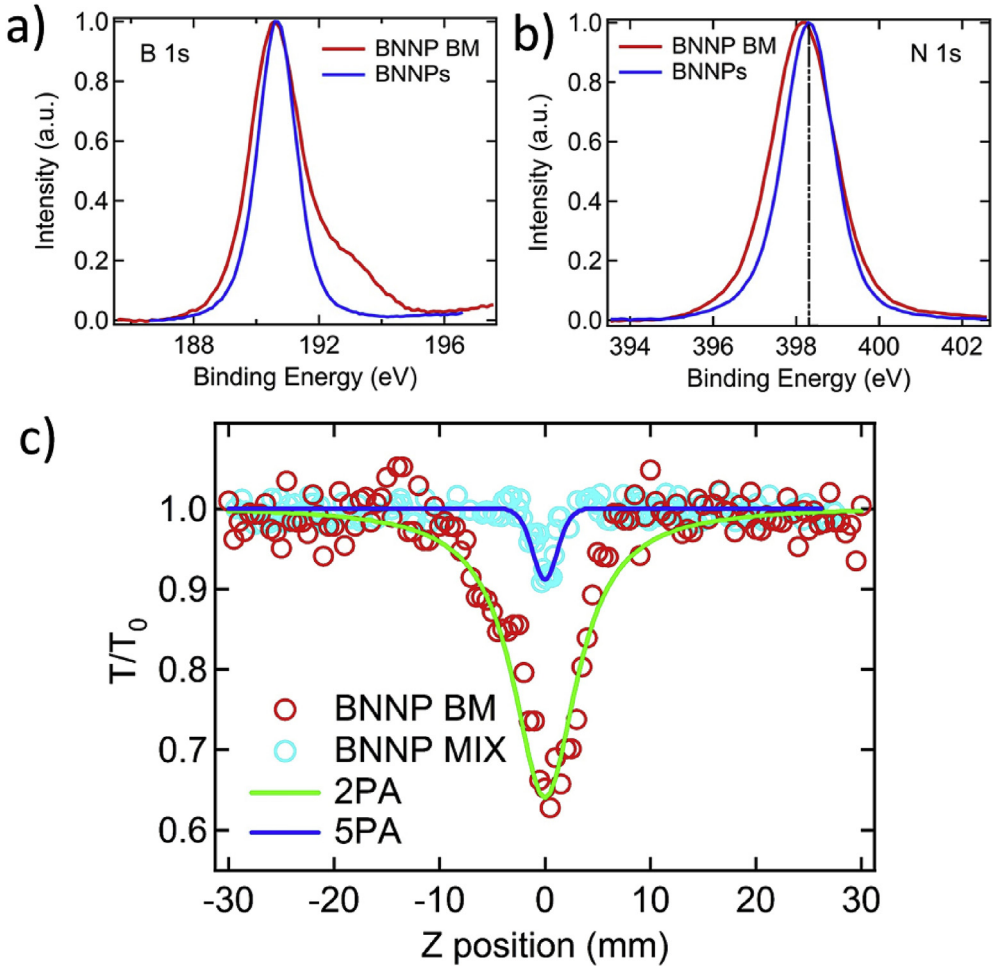

Fig. 4. a) and b) show the XPS spectra of pristine and ball milled BNNPs. A new peak is observed ~193 eV in the B 1s spectrum, which is indicative of B-O bonds or the incorporation O atoms into BN lattice. The N 1s spectrum was found to broaden and downshift by ~0.2 eV possibly due to C doping. c) Z-scan curves for BNNP BM dispersion in IPA, which exhibits a 2PA response (red circles). The mixture of BNNPs and graphite powder, prior to ball milling, exhibited a 5PA response as expected (blue circles). (For interpretation of the references to colour in this figure legend, the reader is referred to the Web version of this article.)

literature values for nitrogen doped graphenes, which may be indicative of boron containing environments [50,51]. They are consistent with nitrogen environments reported for other carbon containing boron nitride systems [48]. Overall, our analysis showed that CBN sample had ~35 at. % carbon (see Supplementary Table 1) suggesting that the sample should exhibit 2PA. Accordingly, we observed that CBN displayed 2PA even at low fluence ~0.2–0.6 J/cm2 (Fig. S8).

We also performed similar studies with ball-milled BN. For ball milling, we mixed BNNPs and graphite in 9:1 wt ratio, which we refer to as "BNNP MIX". The Z-scan curves for BNNP MIX sample (discussed later in Fig. 4c), prior to ball milling, showed a clear 5PA signal intrinsic to BNNPs at a low laser fluence 100 μJ (~0.2 J/cm^2 at the focus). Next, the BNNP MIX sample was ball milled for 2 h for doping O/C into the BN lattice. An extensive characterization toolset including XRD, Raman spectroscopy (Fig. S9) and XPS (Fig. 4) confirmed doping of both O and C atoms (~1–2 at. %, much lower compared to CBN, as evinced from XPS in Fig. 4a and b) in ball milled BNNPs [38,40,49], which we henceforth refer to as BNNP BM sample. As shown in Fig. 4a and b, the B 1s and N 1s spectra from pristine and doped BNNPs show primary binding energies of 190.7 and 398.3 eV, respectively. We observed an extra peak ~192.8 eV in the B 1s spectrum (Fig. 4a), which is known to arise from B—O bonds, confirming O-doping in BNNP BM samples. Furthermore, we also found that the N 1s spectrum was slightly downshifted from ~398.3 to 398.1 eV, which was previously attributed to C—N bonds [38,49]. As shown in Fig. 4c, we observed a 2PA response in the Z-scan curve for BNNP BM sample in IPA even at a low laser energy of 100 μJ (~0.2 J/cm^2 at the focus) while BNNP MIX samples (prior to ball milling) exhibited the intrinsic 5PA response. The values of 2PA coefficients for BNNP BM and photo-transformed BNNPs in IPA were found to be very similar (Table S2). This implies that the mid-gap states supporting a 2PA response in BNNP BM and photo-transformed BNNPs are similar *viz.*, O/C dopant-induced electronic states present ~2–2.5 eV within the band gap of BN (*cf.* inset of Fig. 2b).

5. Conclusions

In summary, we report the discovery of a rarely observed nonlinear phenomenon, *i.e.*, five-photon absorption (5PA) in 2D h-BN nanoplatelets (BNNPs). Through a systematic study we show that the nonlinear optical response of BNNPs dispersed in isopropyl alcohol (IPA) switches from a 5PA to a 2PA response when the laser fluence exceeds 0.6 J/cm^2 (at the focus or $z = 0$) due to photoinduced O/C doping (from IPA) of BNNPs. Previous studies on the nonlinear optical properties of BNNPs (Kumbhakar et al. [22]) used very high laser fluence (~3.9 J/cm^2) and thus failed to uncover the inherent 5PA phenomenon in BNNPs. Our finite-element calculations using COMSOL Multiphysics showed a rapid increase in the temperature of edge sites in BNNPs (> 960 °C) suitable for carbonizing IPA and doping of O/C atoms at edge sites in BNNPs. We associate the observation of a 2PA response at a high laser fluence in BNNPs with to the NLO properties of O/C doped BNNPs. This

correlation was independently confirmed from Z-scan spectra of BNNPs doped with O/C atoms using two-different methods: 1) chemical vapor deposition and 2) ball milling with graphite. While XPS presented clear evidence of heteroatomic bonding in both the CVD and in the ball milled BNNPs, Z-scan spectra at a low laser fluence showed a 2PA response, akin to the Z-scan spectra of photo-transformed BNNPs. Lastly, the 2PA coefficients in ball milled BNNPs and photo-transformed BNNPs were found to be similar, further confirming our hypothesis.

Acknowledgements

R.P. and Y.C.D. would like to thank Drs. Haijun Qian and Longyu Hu for their kind help with the HRTEM image and AFM. R.P., A.M.R thank Dr. Dickey, North Carolina State University for allowing the use of XPS at NCSU. R.P. is thankful to Clemson University for providing start-up grant. W. T. and S. E. thank FWO (G.0C60.13N) and the European Union's European Fund for Regional Development and Flanders Innovation & Entrepreneurship (Accelerate^3 project, Interreg Vlaanderen-Nederland program) for financial support. W. T. also thanks the Provincie West-Vlaanderen (Belgium) for his Provincial Chair in Advanced Materials. R.P. and A. M. R. would like to thank NASA-EPSCoR grant #2022438.

Appendix A. Supplementary data

Supplementary data to this article can be found online at https://doi.org/10.1016/j.optmat.2018.10.022.

References

[1] J. Wang, C.H. Lee, Y.K. Yap, C.Y. Zhi, D. Golberg, Y.K. Yap, S.A. Green, H.Y. Liu, A. Prasad, V.K. Kayastha, Y.K. Yap, F. Ducastelle, A. Loiseau, Recent advancements in boron nitride nanotubes, Nanoscale 2 (2010) 2028, https://doi.org/10.1039/c0nr00335b.

[2] R.V. Gorbachev, I. Riaz, R.R. Nair, R. Jalil, L. Britnell, B.D. Belle, E.W. Hill, K.S. Novoselov, K. Watanabe, T. Taniguchi, A.K. Geim, P. Blake, Hunting for monolayer boron nitride: optical and Raman signatures, Small 7 (2011) 465–468, https://doi.org/10.1002/smll.201001628.

[3] L. Lin, Y. Xu, S. Zhang, I.M. Ross, A.C.M. Ong, D. a. Allwood, Fabrication and luminescence of monolayered boron nitride quantum dots, Small 10 (2014) 60–65, https://doi.org/10.1002/smll.201301001.

[4] A.L. Tiano, C. Park, J.W. Lee, H.H. Luong, L.J. Gibbons, S.-H. Chu, S.I. Applin, P. Gnoffo, S. Lowther, H.J. Kim, P.M. Danehy, J.A. Inman, S.B. Jones, J.H. Kang, G. Sauti, S.A. Thibeault, V. Yamakov, K.E. Wise, J. Su, C.C. Fay, Boron Nitride Nanotube: Synthesis and Applications, SPIE Conf, 2014.

[5] L. Zhibo, Z. Xiaoliang, Y. Xiaoqing, C. Yongsheng, T. Jianguo, Nonlinear optical properties of graphene-based materials, Spec. Issue Graphene August 5723 (2012) 2971–2982, https://doi.org/10.1007/s11434-012-5270-4.

[6] K. Wang, Y. Feng, C. Chang, J. Zhan, C. Wang, Q. Zhao, J.N. Coleman, L. Zhang, W. Blau, J. Wang, Broadband ultrafast nonlinear absorption and nonlinear refraction of layered molybdenum dichalcogenide semiconductors, Nanoscale 6 (2014) 10530–10535, https://doi.org/10.1039/C4NR02634A.

[7] B. Anand, R. Podila, K. Lingam, S.R. Krishnan, S. Siva Sankara Sai, R. Philip, A.M. Rao, Optical diode action from axially asymmetric nonlinearity in an all-carbon solid-state device, Nano Lett. 13 (2013) 5771–5776, https://doi.org/10.1021/nl403366d.

[8] H. Zhang, S.B. Lu, J. Zheng, J. Du, S.C. Wen, D.Y. Tang, K.P. Loh, Molybdenum disulfide (MoS 2) as a broadband saturable absorber for ultra-fast photonics, Optic Express 22 (2014) 7249, https://doi.org/10.1364/OE.22.007249.

[9] Z. Guo, H. Zhang, S. Lu, Z. Wang, S. Tang, J. Shao, Z. Sun, H. Xie, H. Wang, X.-F. Yu, P.K. Chu, From black phosphorus to phosphorene: basic solvent exfoliation, evolution of Raman scattering, and applications to ultrafast photonics, Adv. Funct. Mater. 25 (2015) 6996–7002, https://doi.org/10.1002/adfm.201502902.

[10] Y. Dong, D. Saini, L.A. Echegoyen, R. Podila, Passive optical switches based on endohedral fullerenes, Opt. Mater. (Amst). 53 (2016) 14–18, https://doi.org/10.1016/j.optmat.2016.01.002.

[11] B. Zhu, X. Chen, X. Cui, Exciton binding energy of monolayer WS 2, Sci. Rep. 5 (2014), https://doi.org/10.1038/srep09218.

[12] R.W. Newson, J. Dean, B. Schmidt, H.M. Driel, Van, Ultrafast Carrier kinetics in exfoliated graphene and thin graphite films, Optic Express 17 (2009) 2326.

[13] Q. Bao, H. Zhang, Z. Ni, Y. Wang, L. Polavarapu, Z. Shen, Q.-H. Xu, D. Tang, K.P. Loh, Monolayer graphene as a saturable absorber in a mode-locked laser, Nano Res. 4 (2011) 297–307, https://doi.org/10.1007/s12274-010-0082-9.

[14] A.H. Castro Neto, N.M.R. Peres, K.S. Novoselov, A.K. Geim, The electronic properties of graphene, Rev. Mod. Phys. 81 (2009) 109–162, https://doi.org/10.1103/RevModPhys.81.109.

[15] H. Zhang, S.B. Lu, J. Zheng, J. Du, S.C. Wen, D.Y. Tang, K.P. Loh, Molybdenum disulfide (MoS_2) as a broadband saturable absorber for ultra-fast photonics, Optic Express 22 (2014) 7249, https://doi.org/10.1364/OE.22.007249.

[16] H. Zhang, S. Virally, Q. Bao, L. Kian Ping, S. Massar, N. Godbout, P. Kockaert, Z-scan measurement of the nonlinear refractive index of graphene, Opt. Lett. 37 (2012) 1856, https://doi.org/10.1364/OL.37.001856.

[17] J.M.P. Almeida, D.S. Da Silva, L.R.P. Kassab, S.C. Zilio, C.R. Mendonça, L. De Boni, Universidade de São Paulo Ultrafast third-order optical nonlinearities of heavy metal oxide glasses containing gold nanoparticles Ultrafast third-order optical nonlinearities of heavy metal oxide glasses containing gold nanoparticles, Opt. Mater. (Amst). 36 (2014) 829–832.

[18] C.P. Singh, K.S. Bindra, G.M. Bhalerao, S.M. Oak, Investigation of optical limiting in iron oxide nanoparticles, Optic Express 16 (2008) 8440.

[19] A. Acharya, R. Behera, G.S. Roy, Non-linear characteristic of copper oxide (CuO) through Z-scan technique, Am. J. Phys. Educ. 6 (2012).

[20] F. Ma, M. Wang, Y. Shao, L. Wang, Y. Wu, Z. Wang, X. Hao, Z.F. Wang, K. Storr, L. Balicas, F. Liu, P.M. Ajayan, "Thermal substitution" for preparing ternary BCN nanosheets with enhanced and controllable nonlinear optical performance, J. Mater. Chem. C. 5 (2017) 2559–2565, https://doi.org/10.1039/C7TC00131B.

[21] W.C. Hurlbut, Y.-S. Lee, K.L. Vodopyanov, P.S. Kuo, M.M. Fejer, Multiphoton absorption and nonlinear refraction of GaAs in the mid-infrared, Opt. Lett. 32 (2007) 668.

[22] P. Kumbhakar, A.K. Kole, C.S. Tiwary, S. Biswas, S. Vinod, J. Taha-Tijerina, U. Chatterjee, P.M. Ajayan, Nonlinear optical properties and temperature-dependent UV-vis absorption and photoluminescence emission in 2D hexagonal boron nitride nanosheets, Adv. Opt. Mater. 3 (2015) 828–835, https://doi.org/10.1002/adom.201400445.

[23] S. Webster, S.A. Odom, L.A. Padilha, O.V. Przhonska, D. Peceli, H. Hu, G. Nootz, A.D. Kachkovski, J. Matichak, S. Barlow, H.L. Anderson, S.R. Marder, D.J. Hagan, E.W. Van Stryland, Linear and nonlinear spectroscopy of a Porphyrin – Squaraine – Porphyrin conjugated system, J. Phys. Chem. B 113 (2009) 14854–14867, https://doi.org/10.1021/jp904460f.

[24] Q. Zheng, H. Zhu, S.-C. Chen, C. Tang, E. Ma, X. Chen, Frequency-upconverted Stimulated Emission by Simultaneous Five-photon Absorption, (2013), https://doi.org/10.1038/NPHOTON.2012.344.

[25] W. Chen, S. Bhaumik, S.A. Veldhuis, G. Xing, Q. Xu, M. Grätzel, S. Mhaisalkar, N. Mathews, T.C. Sum, ARTICLE Giant Five-photon Absorption from Multidimensional Core-shell Halide Perovskite Colloidal Nanocrystals, (2017), https://doi.org/10.1038/ncomms15198.

[26] D.H. Friese, R. Bast, K. Ruud, Five-photon absorption and selective enhancement of multiphoton absorption processes, ACS Photonics 2 (2015) 572–577, https://doi.org/10.1021/acsphotonics.5b00053.

[27] S. Kawata, H.-B. Sun, T. Tanaka, K. Takada, Finer features for functional microdevices, Nature 412 (2001) 697–698, https://doi.org/10.1038/35089130.

[28] G. Mainfray, G. Manus, Multiphoton ionization of atoms, Rep. Prog. Phys. 54 (1991) 1333–1372, https://doi.org/10.1088/0034-4885/54/10/002.

[29] E. Van Stryland, M. Sheik-Bahae, Z-scan measurements of optical nonlinearities, Char. Tech. Tabula Org. Nonlinear Mater. (1998) 655–692, https://doi.org/10.1142/S0218863509004671.

[30] M. Sheik-Bahae, A.A. Said, T.-H. Wei, D.J. Hagan, E.W. Van Stryland, Sensitive measurement of optical nonlinearities using a single beam, IEEE J. Quant. Electron. 26 (1990).

[31] T. Woldu, B. Raneesh, P. Sreekanth, M.V. Ramana Reddy, R. Philip, N. Kalarikkal, Size dependent nonlinear optical absorption in BaTiO3 nanoparticles, Chem. Phys. Lett. 625 (2015) 58–63, https://doi.org/10.1016/j.cplett.2015.02.020.

[32] R. Philip, G.R. Kumar, N. Sandhyarani, T. Pradeep, Picosecond optical nonlinearity in monolayer-protected gold, silver, and gold-silver alloy nanoclusters, Phys. Rev. B 62 (2000) 13160–13166, https://doi.org/10.1103/PhysRevB.62.13160.

[33] B. Anand, M. Karakaya, G. Prakash, S.S. Sankara Sai, R. Philip, P. Ayala, A. Srivastava, A.K. Sood, A.M. Rao, R. Podila, Dopant-configuration controlled Carrier scattering in graphene, RSC Adv. 5 (2015) 59556–59563, https://doi.org/10.1039/C5RA05338B.

[34] G. Cassabois, P. Valvin, B. Gil, Hexagonal boron nitride is an indirect bandgap semiconductor, Nat. Photon. 10 (2016) 262–267, https://doi.org/10.1038/nphoton.2015.277.

[35] A. Yamanaka, S. Okada, Energetics and electronic structure of h-BN nanoflakes, Sci. Rep., 30653. doi:10.1038/srep30653.

[36] M. M. Monshi, S.M. Aghaei, I. Calizo, Edge functionalized germanene nanoribbons: impact on electronic and magnetic properties, RSC Adv. 7 (2017) 18900–18908, https://doi.org/10.1039/C6RA25083A.

[37] C. Attaccalite, M. Bockstedte, A. Marini, A. Rubio, L. Wirtz, Coupling of excitons and defect states in boron-nitride nanostructures, Phys. Rev. B 83 (2011), https://doi.org/10.1103/PhysRevB.83.144115.

[38] C. Huang, C. Chen, M. Zhang, L. Lin, X. Ye, S. Lin, M. Antonietti, X. Wang, Carbon-doped BN nanosheets for metal-free photoredox catalysis, Nat. Commun. 6 (2015) 7698, https://doi.org/10.1038/ncomms8698.

[39] L.A. Silva, S.C. Guerini, V. Lemos, J.M. Filho, Electronic and structural properties of oxygen-doped BN nanotubes, IEEE Trans. Nanotechnol. 5 (2006) 517–522, https://doi.org/10.1109/TNANO.2006.880495.

[40] R.S. Singh, Influence of oxygen impurity on electronic properties of carbon and boron nitride nanotubes: a comparative study, AIP Adv. 5 (2015) 117150, https://doi.org/10.1063/1.4936765.

[41] Q. Weng, X. Wang, X. Wang, Y. Bando, D. Golberg, Functionalized hexagonal boron nitride nanomaterials: emerging properties and applications, Chem. Soc. Rev. 45 (2016) 3989–4012, https://doi.org/10.1039/C5CS00869G.

[42] W.-Q. Han, H.-G. Yu, Z. Liu, Convert graphene sheets to boron nitride and boron

nitride?carbon sheets via a carbon-substitution reaction, Appl. Phys. Lett. 98 (2011) 203112, https://doi.org/10.1063/1.3593492.
[43] V.S. Muthukumar, J. Reppert, C.S.S. Sandeep, S.S.R. Krishnan, R. Podila, N. Kuthirummal, S.S.S. Sai, K. Venkataramaniah, R. Philip, A.M. Rao, Optical limiting properties of CdS nanowires, Optic Commun. 283 (2010) 4104–4107, https://doi.org/10.1016/j.optcom.2010.06.020.
[44] B. Anand, R. Podila, P. Ayala, L. Oliveira, R. Philip, S.S.S. Sai, A.A. Zakhidov, A.M. Rao, Nonlinear optical properties of boron doped single-walled carbon nanotubes, Nanoscale 5 (2013) 7271–7276, https://doi.org/10.1039/c3nr01803b.
[45] P. Beiss, R. Ruthardt, H. Warlimont (Eds.), Powder Metallurgy Data. Refractory, Hard and Intermetallic Materials, Springer-Verlag, Berlin/Heidelberg, 2002, , https://doi.org/10.1007/b83029.
[46] S. Chen, P. Li, S. Xu, X. Pan, Q. Fu, X. Bao, Carbon doping of hexagonal boron nitride porous materials toward CO_2 capture, J. Mater. Chem. A. 6 (2018) 1832–1839, https://doi.org/10.1039/C7TA08515J.
[47] S. Beniwal, J. Hooper, D.P. Miller, P.S. Costa, G. Chen, S.-Y. Liu, P.A. Dowben, E.C.H. Sykes, E. Zurek, A. Enders, Graphene-like boron–carbon–nitrogen monolayers, ACS Nano 11 (2017) 2486–2493, https://doi.org/10.1021/acsnano.6b08136.
[48] A. Prakash, K.B. Sundaram, Optical and XPS studies of BCN thin films by co-sputtering of B4C and BN targets, Appl. Surf. Sci. 396 (2017) 484–491, https://doi.org/10.1016/J.APSUSC.2016.10.180.
[49] W. Lei, H. Zhang, Y. Wu, B. Zhang, D. Liu, S. Qin, Z. Liu, L. Liu, Y. Ma, Y. Chen, Oxygen-doped boron nitride nanosheets with excellent performance in hydrogen storage, Nano Energy 6 (2014) 219–224, https://doi.org/10.1016/j.nanoen.2014.04.004.
[50] Y. Zhang, Z. Sun, H. Wang, Y. Wang, M. Liang, S. Xue, Nitrogen-doped graphene as a cathode material for dye-sensitized solar cells: effects of hydrothermal reaction and annealing on electrocatalytic performance, RSC Adv. 5 (2015) 10430–10439, https://doi.org/10.1039/C4RA13224F.
[51] N. Mahmood, C. Zhang, H. Yin, Y. Hou, Graphene-based nanocomposites for energy storage and conversion in lithium batteries, supercapacitors and fuel cells, J. Mater. Chem. A. 2 (2014) 15–32, https://doi.org/10.1039/C3TA13033A.